Characterizing the Diurnal Variability of Convective Available Potential Energy in the Southeastern US

Anthony Freveletti

Department of Earth, Ocean and Atmospheric Science,

Florida State University

Undergraduate Honors Thesis towards fulfillment of Honors in the Major Thesis

Committee Chair: Dr. V. Misra (EOAS)

Committee Member: Dr. Z. Wu (EOAS)

Committee Member: Dr. A. Agashe (Dept. of Mathematics)

Abstract:

This study reports on the analysis of the diurnal cycle of Convectively Available Potential Energy (CAPE) over the Southeastern US (SEUS). The data that is analyzed for CAPE is the Florida Climate Institute-Florida State University Land-Atmosphere Reanalysis for the SEUS (FLAReS1.0), which is a dynamically downscaled product at 10 km grid resolution from ~222 km of NOAA's Centennial global reanalysis. In this study we have examined the monthly climatology of the diurnal cycle in the SEUS over a 20 year period (1986-2005).

The analysis of the diurnal cycles is unique to this study, which involves first conducting an Empirical Orthogonal Functional (EOF) analysis followed by Ensemble Empirical Mode Decomposition (EEMD) to reconstruct the diurnal anomalies of CAPE from the original timeseries. Our analysis reveals that the SEUS exhibits a robust diurnal cycle throughout the year including the Gulf of Mexico. Interestingly, the diurnal maximum of CAPE in the boreal winter season over SEUS is comparable to that in the boreal summer season. Furthermore, CAPE shows significant seasonal variability and high frequency (synoptic) variability in the SEUS.

Table of Contents

Introduction:

Convective available potential energy (CAPE) and convective inhibition (CIN) are characteristics of the environment used to parameterize convective precipitation and assess the likelihood of thunderstorm development and its strength (Riemann-Campe et al. 2008). Both variables relate to the buoyancy of an air parcel between pressure levels, where CAPE denotes the available potential energy that could be released by the convection of positively buoyant air between the level of free convection (LFC) and the equilibrium level (EL) or level of neutral buoyancy, and CIN refers to the amount of energy needed to overcome the negative buoyancy between the surface and the LFC. CAPE is also suggestive of the instability in the atmospheric layer as convection tries to remove this layer of 'critical' positive buoyancy, which otherwise will build ad infinitum and make the atmospheric column highly unstable to remain stacked as a column. Higher CAPE values indicate a more unstable layer or more positively buoyant parcels; thus, greater CAPE values mean deeper convection, a greater chance of thunderstorm development, and higher updraft speeds. Higher CIN indicates more substantial thunderstorm development suppression as parcels need more energy to break through the cap. Both CAPE and CIN are determined primarily by thermodynamic variables of temperature and moisture in the atmosphere. However, a multitude of factors determines the evolution of these variables, such as soil moisture, cloud cover, radiation and surface enthalpy fluxes, and atmospheric circulation (Riemann-Campe et al. 2008; Graf et al. 2021).

CIN is calculated through the ascent of the parcel from its origin to the LFC and thus relays how much energy is needed for the parcel to rise to the LFC. In other words, CIN is the amount of energy to overcome for convection to occur. Therefore, even with high values of CAPE, if enough energy is not supplied to the parcel to overcome the CIN barrier, extreme weather (associated with

strong convection) cannot develop. In an environment where the CIN is weak, moderate surface heating, boundary layer moistening, or orographic lifting is generally enough to overcome this barrier and give rise to convection. Subsequently, in an environment with higher amounts of CIN, the CAPE continues to develop and strengthen till fast, deep convection overcomes CIN, usually resulting in powerful thunderstorms by releasing the throttled CAPE. However, too much inhibition will suppress convection altogether and inhibit cloud formation (Rasmussen et al. 2017).

Given the importance of CAPE and CIN to the outbreak of atmospheric convection, there is significant interest in understanding their spatial and temporal variations. Doing so can potentially help in understanding the variations of severe weather like thunderstorms and tornado outbreaks in a region like the Southeastern US. In this work, we focus on the diurnal variation of CAPE.

Due to the strong influence of temperature and moisture on CAPE, its diurnal cycle often peaks during the late afternoon when there has been sufficient surface heating and is lowest at night when the solar radiation received at the surface lessens. However, this diurnal cycle of CAPE is not always the case owing to variations in the local moisture content and or variations of temperature/moisture as it relates to the circulation, which can alter the diurnal cycle of CAPE. CIN, in contrast, usually peaks in the late evening-early morning period and reaches its minimum during the mid-afternoon (Zhang 2008). This diurnal cycle of CIN is implied by the radiative cooling taking place overnight. Radiative cooling causes a strong temperature inversion near the surface, which usually maximizes in the late evening - early morning, thus maximizing CIN. Like CAPE, the variations of temperature and moisture contribute to changes in the diurnal behavior of CIN.

As shown in Fig. 1, the SEUS is a region prone to many Billion Dollar disasters like landfalling tropical cyclones, tornado outbreaks, severe thunderstorms, droughts, freeze events, flooding, etc. Some of these events are associated with the evolution of CAPE, like tornado outbreaks and severe thunderstorms, warranting the study of these parameters. Incidentally, the SEUS is also a region that exhibits large rainfall variability (e.g., Selman and Misra 2015; Misra et al. 2017). Rainfall heavily impacts the surrounding environment, as it consumes large amounts of energy and moistens the soil, both of which are contributing factors to the temperature and moisture and, thus, the CAPE's magnitude. Since climatologically, the SEUS is the wettest region in the US, a noticeable conclusion is that the variations of CAPE and CIN must also be robust. The effects of irrigation further exacerbate this. As shown by Saeed et al. (2009), irrigation increases the amount of local precipitation through evapotranspiration which also induces a second-order effect on atmospheric circulation and the strengthening of tropical rain belts (e.g., Selman and Misra 2015; Misra et al. 2017).

This study's data is obtained from DiNapoli and Misra (2012). They have reconstructed over 100 years (1901-2008) of atmospheric reanalysis over the SEUS by dynamically downscaling a global atmospheric reanalysis at 2° (~222 km) to 10 km grid spacing. We use this extensive data to examine the diurnal variations of CAPE in SEUS and understand how these diurnal variations may vary seasonally. This gridded dataset of meteorological variables over the SEUS provides a unique opportunity to examine the low-frequency variations of diurnal variability of CAPE.

Methodology:

In order to obtain the diurnal variability of CAPE, we must first obtain their values. Mathematically, CAPE is defined as:

$$CAPE = g \int_{LFC}^{EL} \frac{(T_V' - T_V)}{T_V} dz ------(1)$$

where T'v is the virtual temperature of the parcel, Tv is the virtual temperature of the environment, and g is the acceleration due to gravity. For CAPE, the formula is integrated from the LFC to the EL. Visualized on a thermodynamic diagram, this represents the area between the lifted parcel and the environmental temperature. It is often relevant to consider parcels of different origins, thus, multiple types of CAPE exist such as: mixed-layer (MLCAPE), most unstable (MUCAPE), and surface-based (SBCAPE), etc. In this study MUCAPE was calculated, wherein the most unstable parcel in the lowest 300 km was chosen to be lifted. Likewise, CIN is determined by Eq. (2), which differs from Eq. (1) in the bounds in the integral range from the Surface up to the LFC.

$$CIN = g \int_{Surface}^{LFC} \frac{(T_V' - T_V)}{T_V} dz ------(2)$$

Graphically, CIN is depicted as the negative area between the environmental temperature and the dry/moist adiabat being followed by the parcel. Since the environmental temperature is warmer than the parcel, this indicates a stable layer and thus the amount of energy needed to be overcome by the parcel to reach the LFC.

All calculations of CAPE were done in Fortran using the program provided by the National Center for Atmospheric Research (NCAR). There was, however, one issue that arose during these calculations. The program utilized the Newton-Raphson method to determine the pressure level of the LCL, but there were occasional situations where there was a "lack of convergence" to this pressure level. Thus, files that encountered this issue produced no data. Instead of skipping over these files, all values in the grid were assumed to be zero. This was done because the method used for determining the diurnal variability relies on continuous data to function properly. A normalized plot of the CAPE values for a single, arbitrary grid point were then plotted for a few chosen years to check for any abnormalities (Fig. 2).

Following this computation, is the assessment of their temporal and spatial variabilities. To do this, Empirical Orthogonal Functions (EOF) and Ensemble Empirical Mode Decomposition (EEMD) were used (EEMD; Wu and Huang 2009). The EOFs of our data are the first to be determined. According to Huug van den Dool (2011), if we have a dataset that varies in space (s) and time (t): X(s,t), we can separate this dataset into two components

$$X(s,t) = \sum_k a_k(t)e_k(s) \quad (3)$$

where k is the mode. For this equality to hold true in Eq. (3), a sufficient number of modes must be summed over; additionally, both functions ak(t) and ek(s) are orthogonal as long as k≠m.

$$\sum_t a_k(t)a_m(t) = 0 \quad (4)$$

$$\sum_s w(s)e_k(s)e_m(s) = 0 \quad (5)$$

In Eq. (5), w(s) is the weighting term that varies depending on the grid. Finally, after some manipulation of the equations, two orthogonality relationships are derived.

$$e_k(s) = \sum_t a_k(t)\, X(s, t) / \sum_t a^2_k(t) \quad (6)$$

$$a_k(t) = \sum_s w(s) e_k(s) X(s, t) / (\sum_s w(s) e^2_k(s)) \quad (7)$$

These state that the spatial distribution of a single mode can be determined from the projection of our data X(s,t) onto the time series of that mode and, through the projection of our data onto the space pattern, the time series of that mode can be determined (Huug van den Dool 2011). Applying this concept to our dataset, we attain

$$X_{S\times T} = (EOF)_{S\times E}(PC)_{E\times T} \quad (8)$$

where EOF is the space component (S), the principal component (PC) is the time component (T), and the subscript "E" refers to the eigenvalue or mode. Thus, the equation states that the EOF multiplied by the PC, with both summed over "E" eigenvalues, equates to the dataset.

An EEMD analysis of the obtained PCs was then computed to isolate the diurnal variations in the timeseries of the PC. EEMD is a data-adaptive signal processing technique, improved from Empirical Mode Decomposition (Huang et al. 1998). This process takes the time series component and decomposes it into complete sets of near orthogonal components called Intrinsic Mode Functions (IMFs). Through this decomposition process, the trend of the time series is determined. However, issues reside in IMFs calculated in the traditional EMD approach termed "mode mixing" (Wu and Huang 2009). EEMD rectifies this issue by doing ensemble runs with differing Gaussian white noise added at each iteration. The mean of these ensembles is computed, and the white noise is substantially reduced, providing a more accurate estimate of the signal within the time series. The diurnal IMF of each PC was then multiplied by the EOFs to recreate the diurnal anomalies ($RCAPE_d$). Mathematically this may be written as:

$$RCAPE_d = (EOF)_{SXE}(PC^F)_{EXT} - - - - - - - - - - (9)$$

Where, $(EOF)_{SXE}\ and\ (PC^F)_{EXT}$ are the EOFs and filtered PCs that isolates the diurnal component for all E (=20) components.

Data description:

The data used in this study was calculated from the Florida Climate Institute-Florida State University Land-Atmosphere Reanalysis for the SEUS (FLAReS1.0; DiNapoli and Misra 2012). The data, originating from the 20th Century Reanalysis (20CR; Compo et al. 2011), was dynamically downscaled from a horizontal resolution of approximately 222 km (~2°) by using the Regional Spectral Model (RSM) at 10 km grid resolution for the years 1901-2008 (DiNapoli and Misra 2012). 222 km is a relatively coarse spatial resolution to obtain accurate local thermodynamic variables and represent coastal regions, which are relatively long in the SEUS, therefore, necessitating a downscaling such as that done in FLAReS1.0. The dataset's domain includes 241 × 236 grid points, with an approximate latitude and longitude range of 16°N to 38°N and 74°W to 100°W, respectively (Fig.1). The meteorological surface variables of temperature, dewpoint temperature, and pressure, were each stored at a 1-hour resolution, and the whole atmosphere was stored every three hours. While FLAReS1.0 may fail to live up to an idealized reanalysis that assimilates strictly observational data, the fidelity was extensively analyzed by DiNapoli and Misra (2012) through multiple validation techniques. DiNapoli and Misra (2012) showed that FLAReS1.0 was consistent with the low-frequency variability produced by ENSO (El Nino Southern Oscillation), AMO (Atlantic Multidecadal Oscillation), and PDO (Pacific Decadal Oscillation), increasing the confidence of the dataset for its use in further studies.

Results:

Fig. 3 shows the average CAPE values at every grid point for a given year. Per year, the spatial variability of CAPE is easily seen through the gradient between the Gulf of Mexico and the SEUS. For example, in 1994, the annual mean values of CAPE in the Gulf ranged from 100-200 J/kg, whereas average values over the SEUS ranged from 0-50 J/kg. Since the plot is the annual mean value, it is impossible to see the temporal variability over the year. However, looking between plots of CAPE for different years allows for this exact kind of assessment for the existence of interannual variability. The year to year variations of CAPE is evident in Fig. 3 with the Gulf of Mexico showing far higher variability than say, Yucatan Peninsula.

To further examine the spatial variance the first 20 EOFs from the 20 years of FLAReS1.0 dataset are plotted in Fig. 4. These EOF patterns show significant spatial heterogeneity that are markedly different from each other. The corresponding PCs of these 20 EOFs are shown in Fig. 5. These PCs exhibit the temporal variability as opposed to the spatial variability in EOF. The variance explained by each of the PCs is shown in Fig. 6. The first 20 PCs explain a total of 22.37% with the first PC explaining 6.5% and the remaining PCs explaining the rest of the 19 PCs explaining 15.87%. Although with 20 PCs the explained total variance is 22.37%, it still is significant considering the significant spatio-temporal variations of CAPE.

As an illustration, we show the 16 IMFs of the first PC in Fig. 7. These IMFs represent distinct temporal variations embedded in the first PC shown in Fig. 5. The EEMD technique has essentially decomposed the temporal variations of the PCs to distinct temporal scales with IMF2 through 16 scaling from higher to lower frequency timescales. The number of IMFs is

approximately determined by log2(length of timeseries) = log2(7307) ~ 13. We produced 16 IMFs of which the first IMF is the original timeseries.

The IMF3 in Fig. 7 is the diurnal component of PC1 of CAPE. To better observe the diurnal signal in IMF3, Fig. 8 shows IMF3 for PCs 1, 10, and 20 over the first five days of every month averaged over all 20 years. Due to the short time scale (five days) over which they were plotted, it is easy to see the maximum and minimum values of diurnal CAPE for every day (Fig. 8).

Fig. 9 depicts the reconstructed diurnal component of CAPE ($RCAPE_d$) following Eq. (9) for specific locations in SEUS marked in Fig. 4 for the boreal summer season (June-July-August). In Fig. 9 the time on the x-axis is in Local Solar Time (LST). Fig. 9 shows that diurnal maximum of CAPE in the summer is around 0900, 1000, 0700, 1200and 0600 LST in Miami, Atlanta, Raleigh, Baton Rouge, and Oxford, respectively. The timeseries in Fig. 9 for these five locations appears deterministic because of the averaging that is done over the 20 summer seasons. However, by averaging the diurnal cycle in Fig. 9 the depicted climatological diurnal cycle for the summer season is unresolved. The values for the June, July, and August season, averaged over 20 years in Fig. 9, however shows spatial variability between locations. At the Southernmost location, Miami, the maximum anomaly occurred just after 9 AM. While we normally observe the largest CAPE values in the late afternoon, it is possible that after some build-up in the morning, the CAPE was used up through precipitation or convection, which would cause CAPE values to decrease as the day continued, leading to the minimum value observed in the afternoon. A similar pattern is shown at the other locations, with Baton Rouge, LA having the latest time of the maximum anomaly, still earlier in the afternoon than one might expect. Furthermore, there is a significant difference in the magnitude of the anomalies between locations. Of the 5, Atlanta and Miami had the largest values

of diurnal CAPE. Coincidentally, both locations also had the lowest values of diurnal CAPE, implying that in the JJA season, there was significant diurnal variability of CAPE in these regions.

Figures 10-14 exhibit the time at which the diurnal maximum of CAPE occurred for every day in every month for locations indicated in Fig. 9. While the time of occurrence is weighted toward the later half of the day, except for a limited number of months, what these plots demonstrate is the dynamic nature of diurnal CAPE. For any given day, the diurnal maximum could occur at nearly any time. For example, in months of June, July, and August the majority distribution of occurrence of diurnal maximum is in the later half of the day, which is unlike the climatological average of the diurnal cycle shown in Fig. 9. In other words, Figs. 10-14 suggest temporal variations of the diurnal cycle that span from high frequency (synoptic to intraseasonal variations) to low frequency (seasonal variations).

Fig. 15 depicts the climatological monthly maximum diurnal CAPE to occur at every grid point, averaged over 20 years. These maximum values vary from month to month (suggesting the climatological seasonal), with a few locations showing less variance than others. The Yucatan Peninsula is an area of relatively high diurnal CAPE year-round, especially in Summer, when the values considerably intensify. In the winter months, diurnal CAPE decreases; however, it still shows some locations of large values like the SEUS . Another area showing substantial variability is the belt stretching from Louisiana to South Carolina. The maximum values in this belt peak during Winter and Spring and decrease to near zero in June before they go over 100 J/kg is months of July and August. Incidentally, the tornado season in the SEUS spans from January to May (Misra 2020), which seemingly matches with the areas of maximum diurnal CAPE. Similar to Fig. 15, Fig. 16 shows the diurnal minimum of CAPE. The diurnal variability is generally weaker across

the domain in the winter relative to the summer season. However, the domain exhibits a robust diurnal variation of CAPE.

Conclusion:

An unprecedented study of CAPE computed at a 3-hourly interval, for 20 years (1985-2004), over the SEUS at 10km grid resolution was conducted. A novel methodology to isolate diurnal variations in CAPE was adopted, which included first conducting an EOF analysis and picking the top 20 PCs in explained variance for conducting EEMD on them. Thereafter, diurnal anomalies of CAPE are reconstructed by multiplying the EOFs with the diurnal component of each PC isolated from EEMD. The diurnal analysis of the gridded CAPE reveals a robust diurnal variability of CAPE across the SEUS and that this diurnal variability exhibits substantial seasonal and high-frequency variations. However, we should note some caveats of this study including the fact that FLAReS1.0 is essentially a model product obtained by downscaling a global reanalysis with a regional atmospheric model. But the availability of the full atmospheric data at 3 hourly interval to compute CAPE is convenient and necessary for such comprehensive analysis. Furthermore, DiNapoli and Misra (2009) have examined more comprehensively the fidelity of the downscaled integration, which encouraged us to conduct this analysis.

Future Work:

In future work, we will include CIN in the diurnal analysis to better look at the overall picture, as CIN plays a vital role in the variance of CAPE and is an essential quantity in the determination of severe weather. Additionally, we would like to do an in-depth verification of the results obtained in this study so that future work can be conducted using the same methodology.

This study will also be extended to 100 years instead of 20 so that decadal and secular variations of diurnal CAPE and CIN can be analyzed.

References:

Compo, G. P., et al. 2011: The twentieth century reanalysis project. *Q J R Meteorol Soc*, **137**, 1-28. https://doi.org/10.1002/qj.776

Graf, M., Arnault, J., Fersch, B., and Kunstmann, H., 2021: Is the soil moisture precipitation feedback enhanced by heterogeneity and dry soils? A comparative study. *Hydrological Processes*, **35**, e14332. https://doi.org/10.1002/hyp.14332

Huang Norden E., and Coauthors, 1998: The empirical mode decomposition and the Hilbert spectrum for nonlinear and non-stationary time series analysis, *Proc. R. Soc. Lond. A.*, **454**, 903–995, http://doi.org/10.1098/rspa.1998.0193

Misra, V., 2020: Regionalizing Global Climate Variations: A Study of the Southeastern US Regional Climate. Elsevier, 324 pp, ISBN:978-0-12-821826-6.

Misra, V., DiNapoli, S. M., Bastola, S., 2012: Dynamic downscaling of the twentieth-century reanalysis over the southeastern United States, *Reg. Environ. Change*, **13**, 15-23, https://doi.org/10.1007/s10113-012-0372-8.

Misra, V., Michael, J.-P., Boyles, R., Chassignet, E. P., Griffin, M., & O'Brien, J. J., 2012: Reconciling the Spatial Distribution of the Surface Temperature Trends in the Southeastern United States, *Journal of Climate*, **25**, 3610-3618. https://doi.org/10.1175/JCLI-D-11-00170.1

Rasmussen, K.L., and Coauthors, 2017: Changes in the convective population and thermodynamic environments in convection-permitting regional climate simulations over the United States. *Clim Dyn,* **55**, 383–408, https://doi.org/10.1007/s00382-017-4000-7

Riemann-Campe, K, Fraedrich, K., and Lunkeit, F., 2008: Global CLimatology of Convective Available Potential Energy (CAPE) and Convective Inhibition (CIN) in ERA-40 reanalysis, *Atmospheric Environment*, **93**, Issues 1-3, 534-545, https://doi.org/10.1016/j.atmosres.2008.09.037.

Saeed, F., Hagemann S., Jacob, D., 2009: Impact of irrigation on the South Asian summer monsoon. *Geophys Res Lett*, **36**, https://doi.org/10.1029/2009GL040625

Zhang, G. J., 2003: Roles of tropospheric and boundary layer forcing in the diurnal cycle of convection in the U.S. southern great plains, *Geophys. Res. Lett.*, **30**, 2281, https://doi.org/10.1029/2003GL018554.

Huug van den Dool, NOAA, 2011: An Iterative Projection Method to Calculate EOFs Successively without Use of the Covariance Matrix. https://www.nws.noaa.gov/ost/climate/STIP/36CDPW/36cdpw-vandendool.pdf

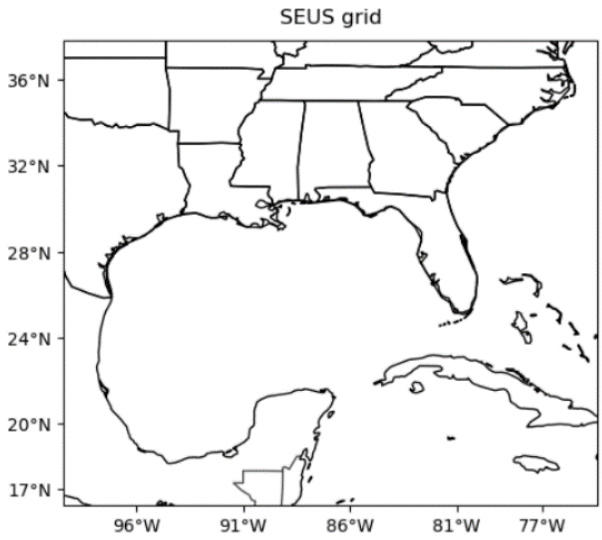

Figure 1: The domain of FLAReS1.0 over which the analysis of this study was conducted and is referred as Southeastern US (SEUS).

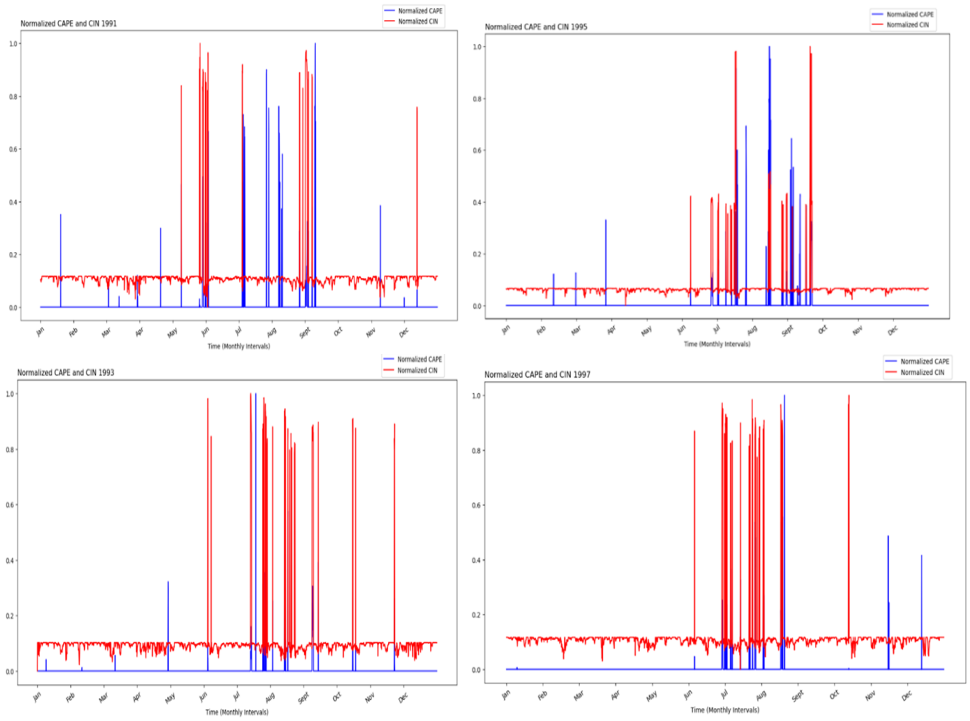

Figure 2: Normalized CAPE and CIN values for the entire year, computed for a single, arbitrary grid point for chosen years.

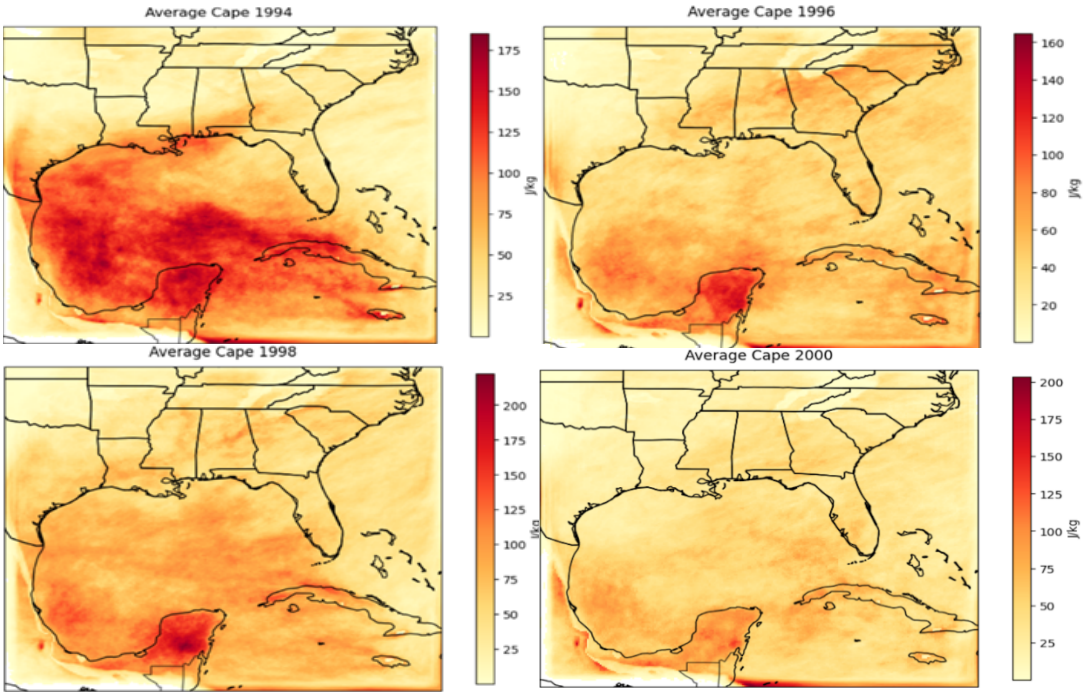

Figure 3: The annual mean values of CAPE for some chosen years over the SEUS domain from FLAReS1.0.

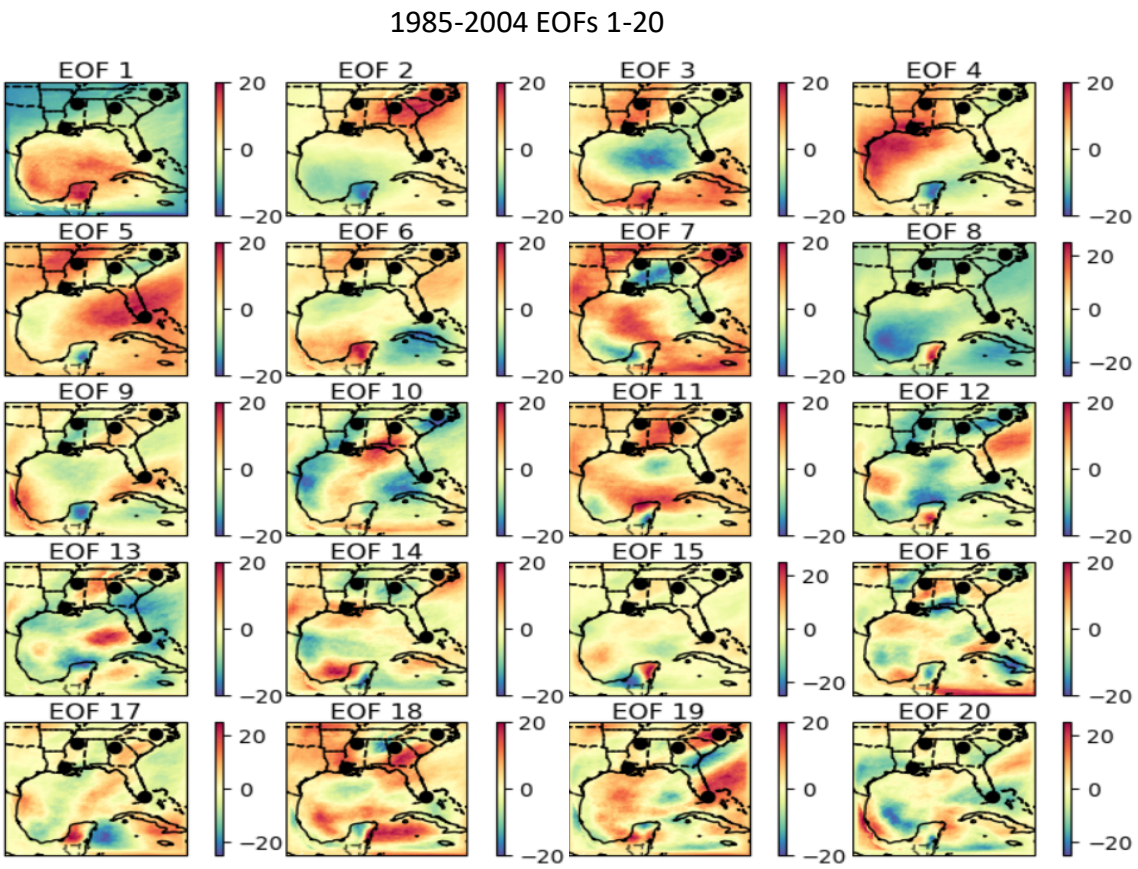

Figure 4: The first 20 Empirical Orthogonal Functions (EOFs) of CAPE from FLAReS1.0 analyzed over the period 1985-2004. The black dots mark stations over which the diurnal cycle time series is shown in Figs. 9 and 10-14.

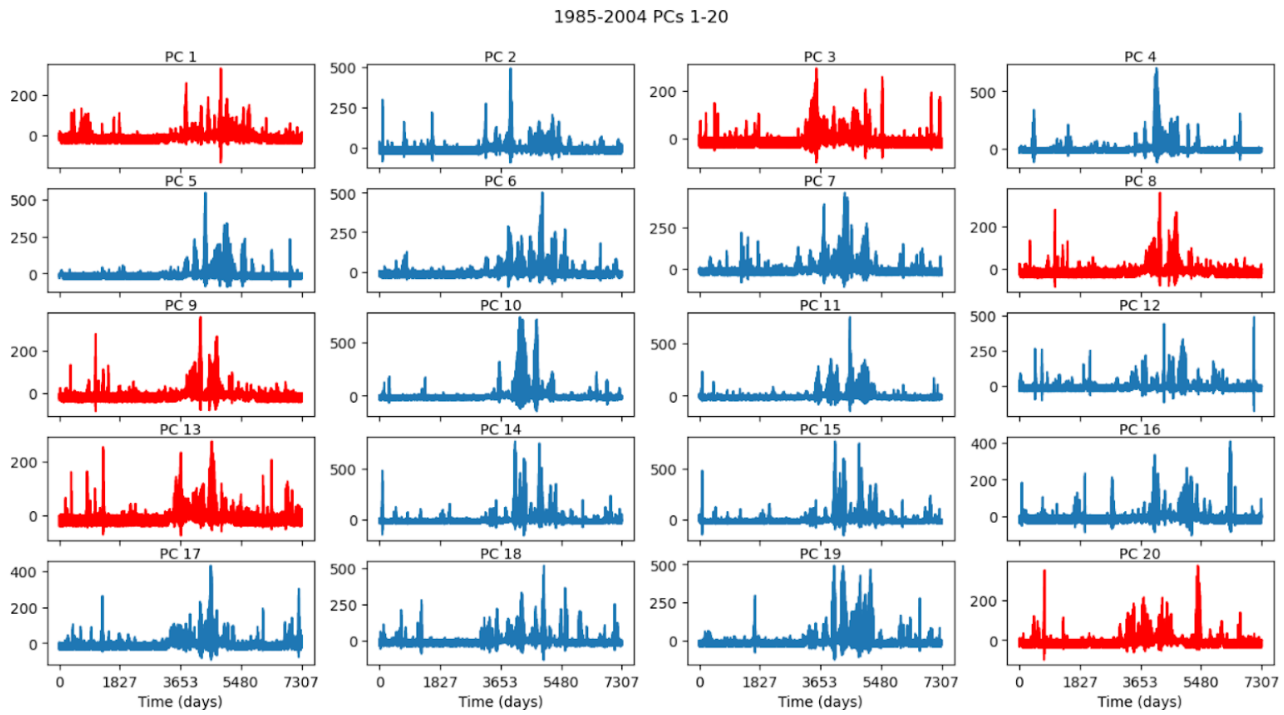

Figure 5: The corresponding Principal Components (PCs) of the EOF's of CAPE from Fig. 4.

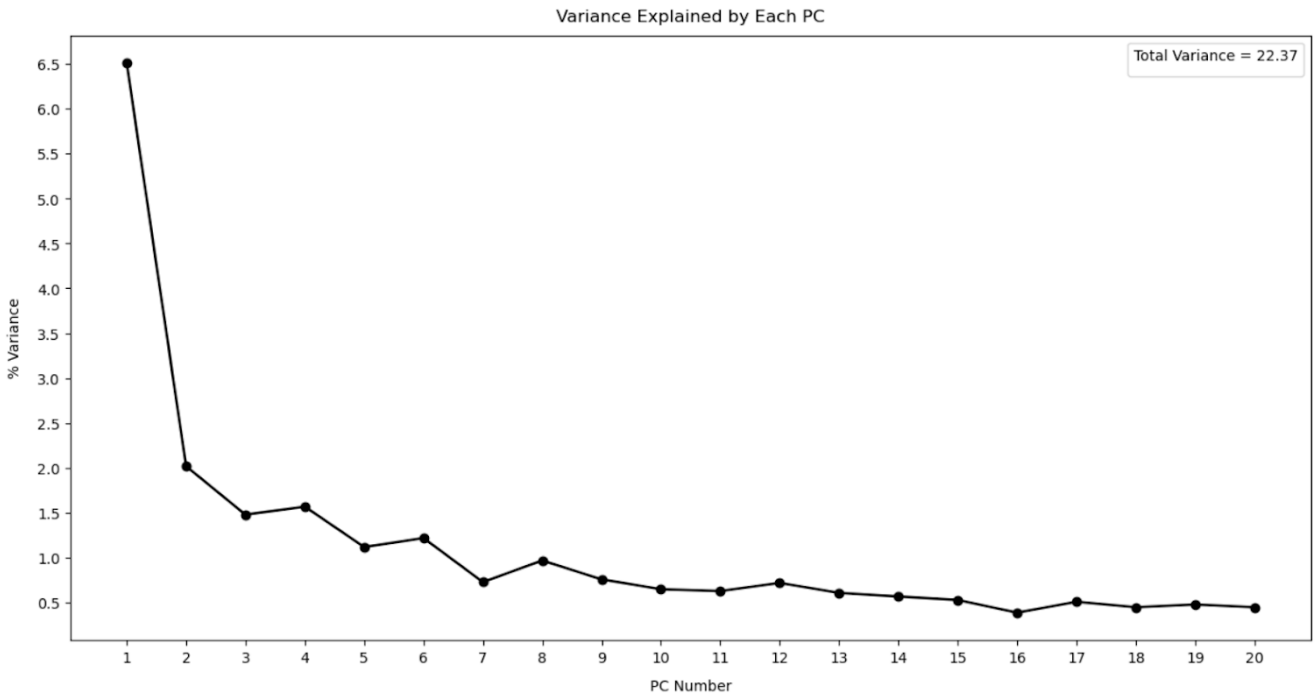

Figure 6: The percent variance explained by the first 20 PCs of CAPE (shown in Fig. 5) from FLAReS1.0.

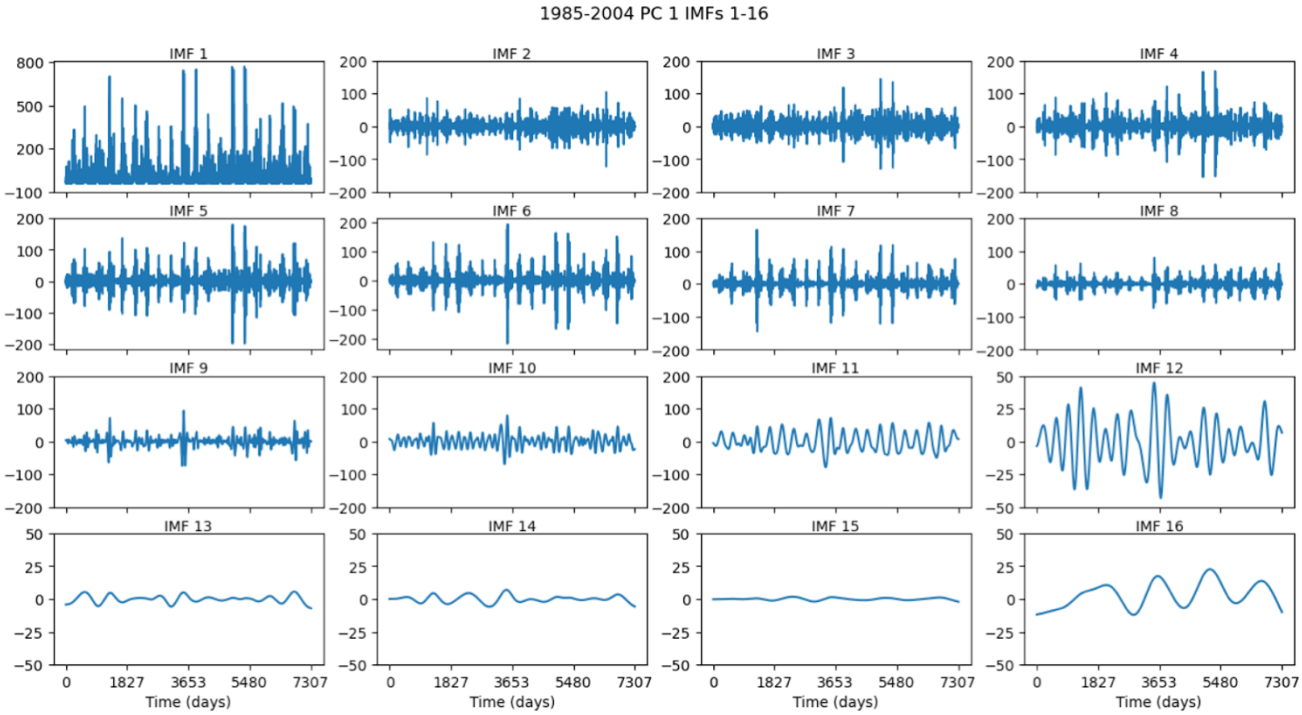

Figure 7: All 16 Intrinsic Mode Functions (IMFs) of the first Principal Component (PC) of CAPE from FLAReS1.0.

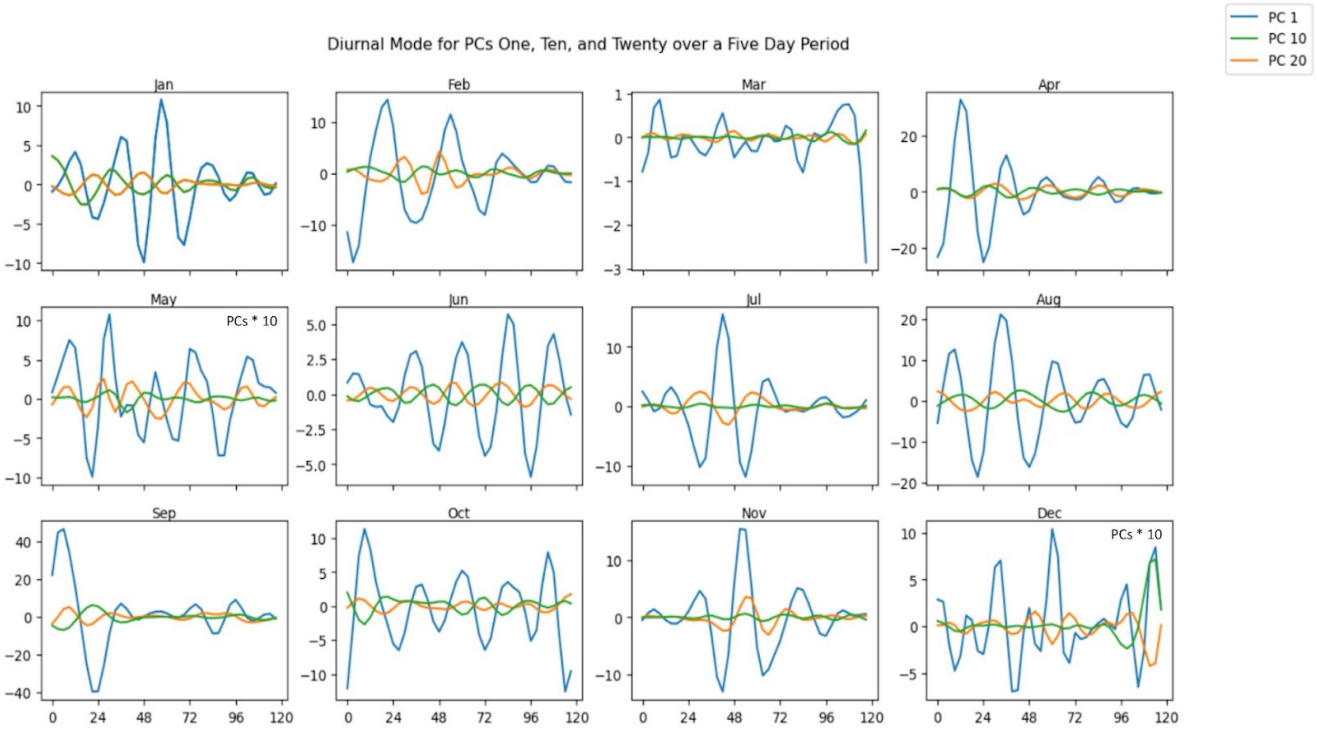

Figure 8: An illustration of the Intrinsic Mode Function (IMF) that isolates the diurnal signal in PCs 1, 10 and 15 shown in Figure 2.

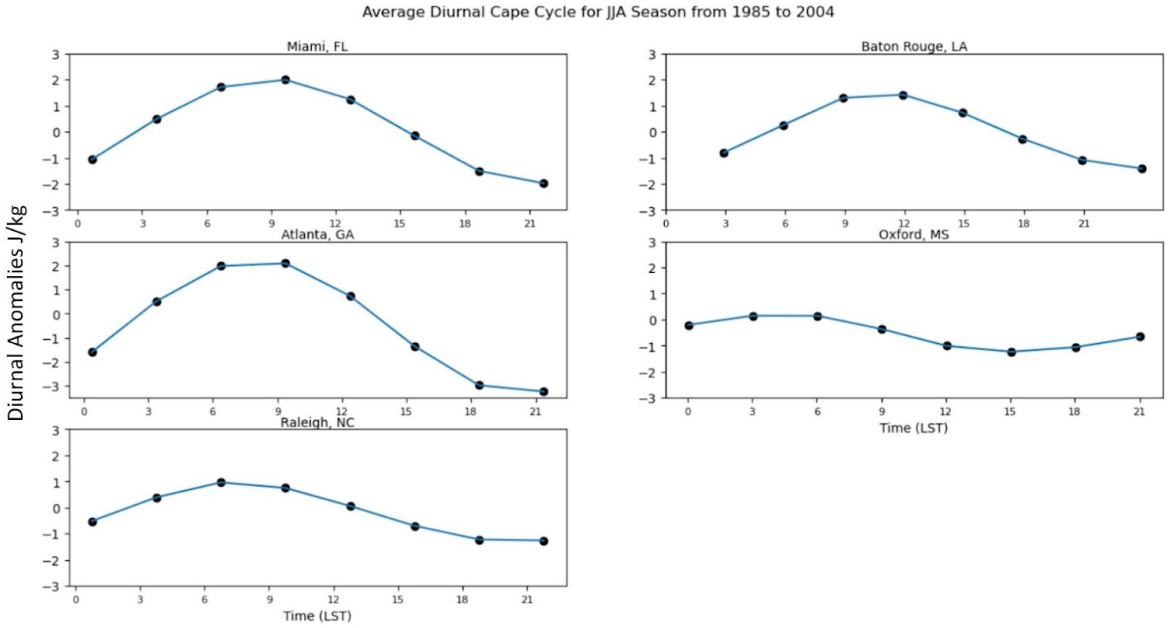

Figure 9: The climatological seasonal (June-July-August) mean diurnal cycle of CAPE from the reconstructed data for selected stations shown in Fig. 4.

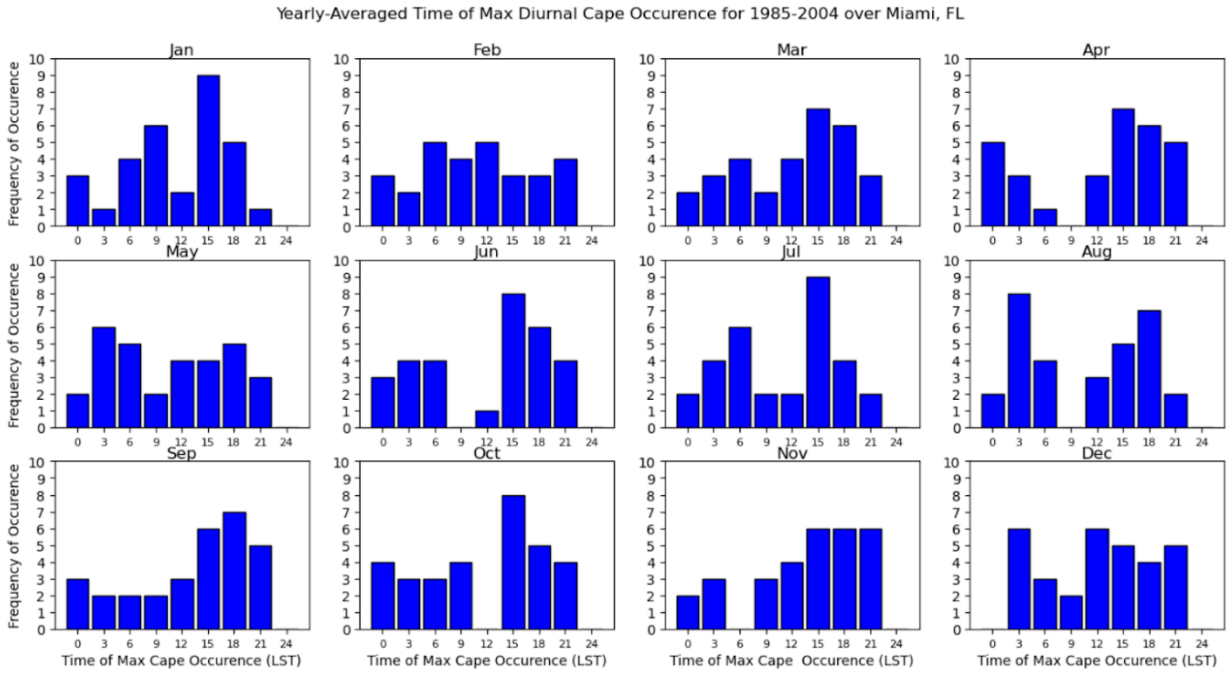

Figure 10: The time of day at which the maximum diurnal CAPE value occurred for every day of the month averaged over 20 years for Miami, Florida.

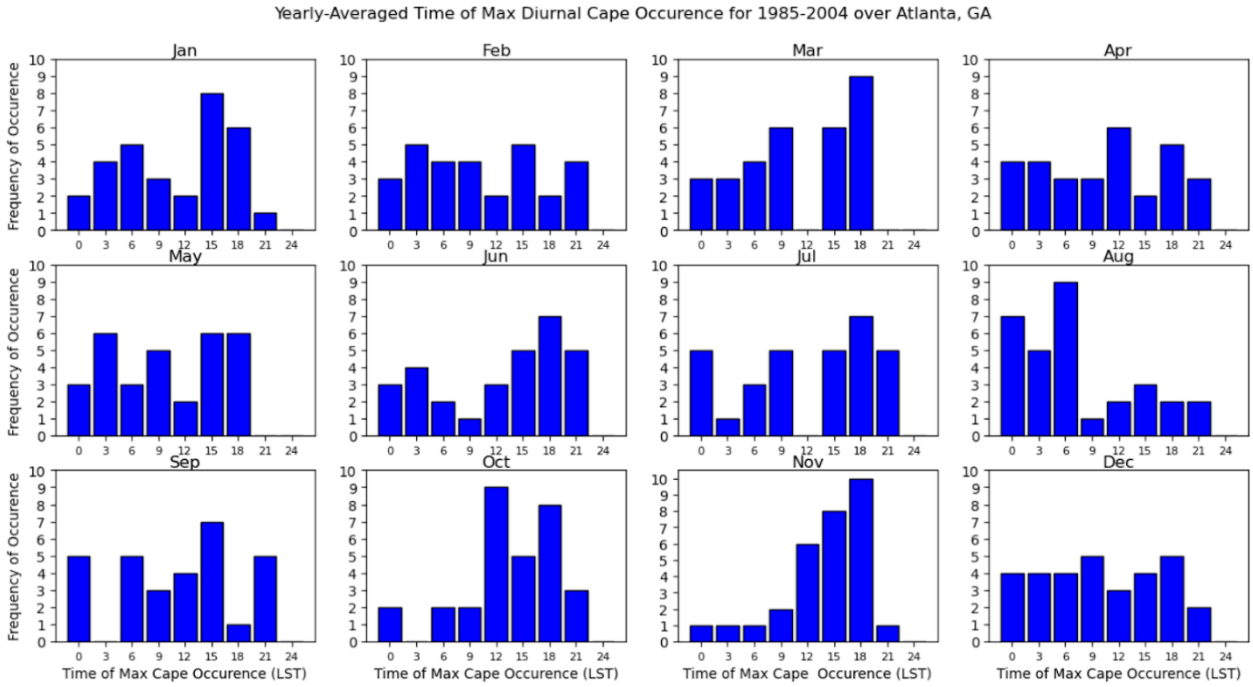

Figure 11: The time of day at which the maximum diurnal CAPE value occurred for every day of the month averaged over 20 years for Atlanta, Georgia.

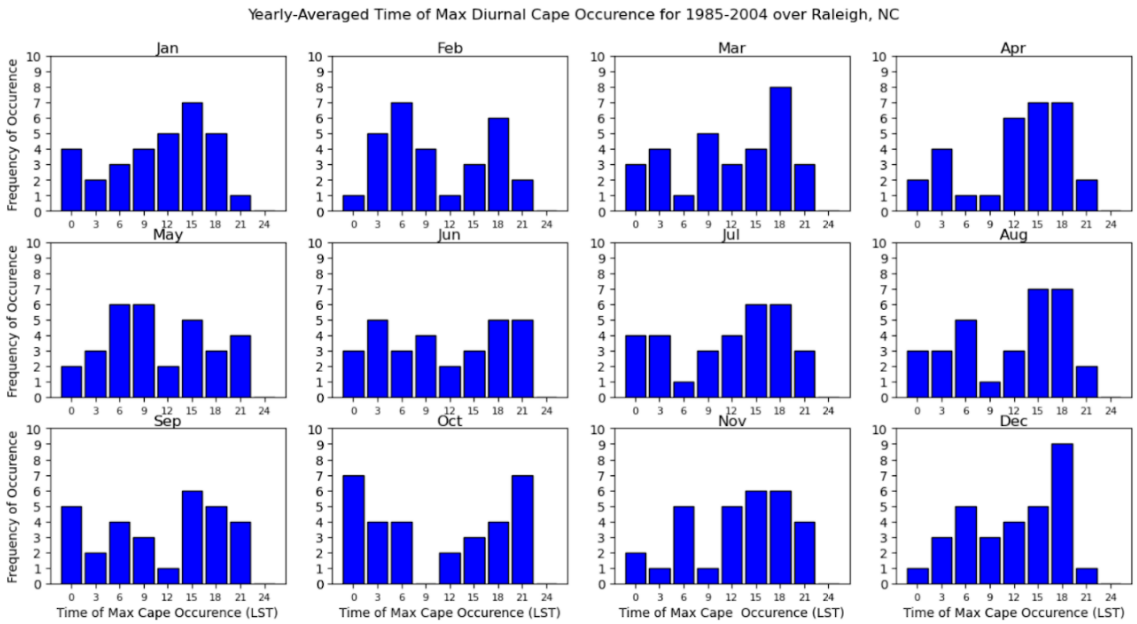

Figure 12: The time of day at which the maximum diurnal CAPE value occurred for every day of the month averaged over 20 years for Raleigh, North Carolina.

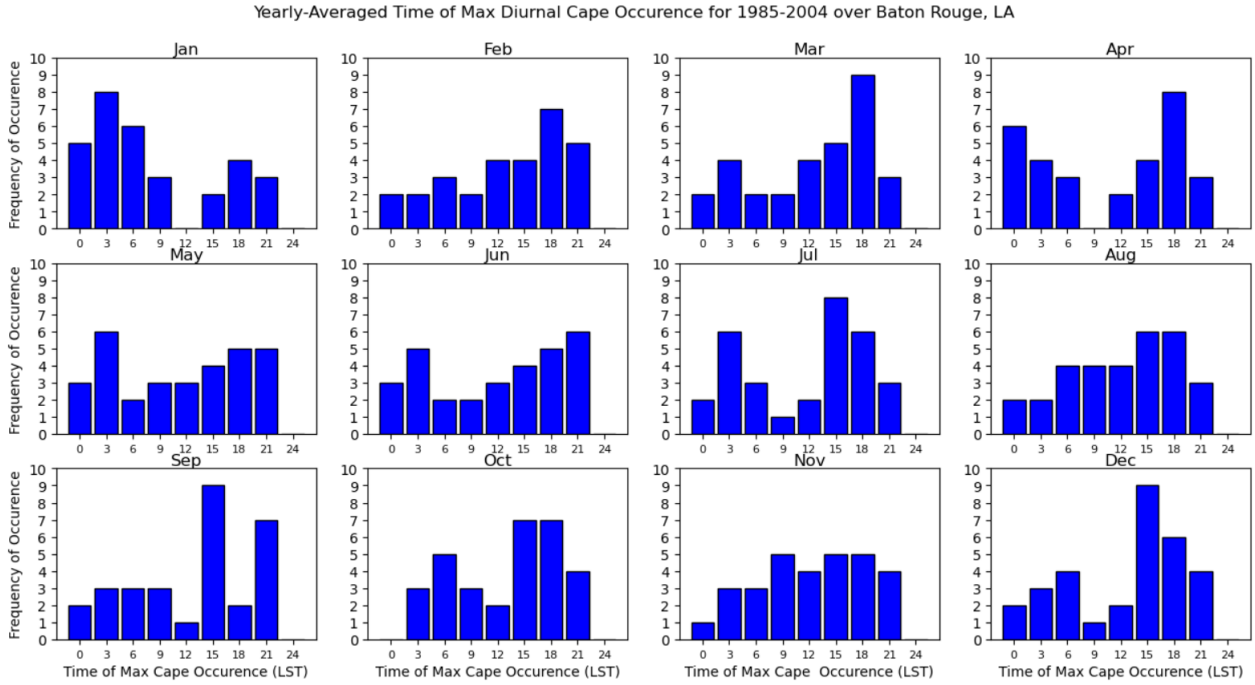

Figure 13: The time of day at which the maximum diurnal CAPE value occurred for every day of the month averaged over 20 years for Baton Rouge, Louisiana.

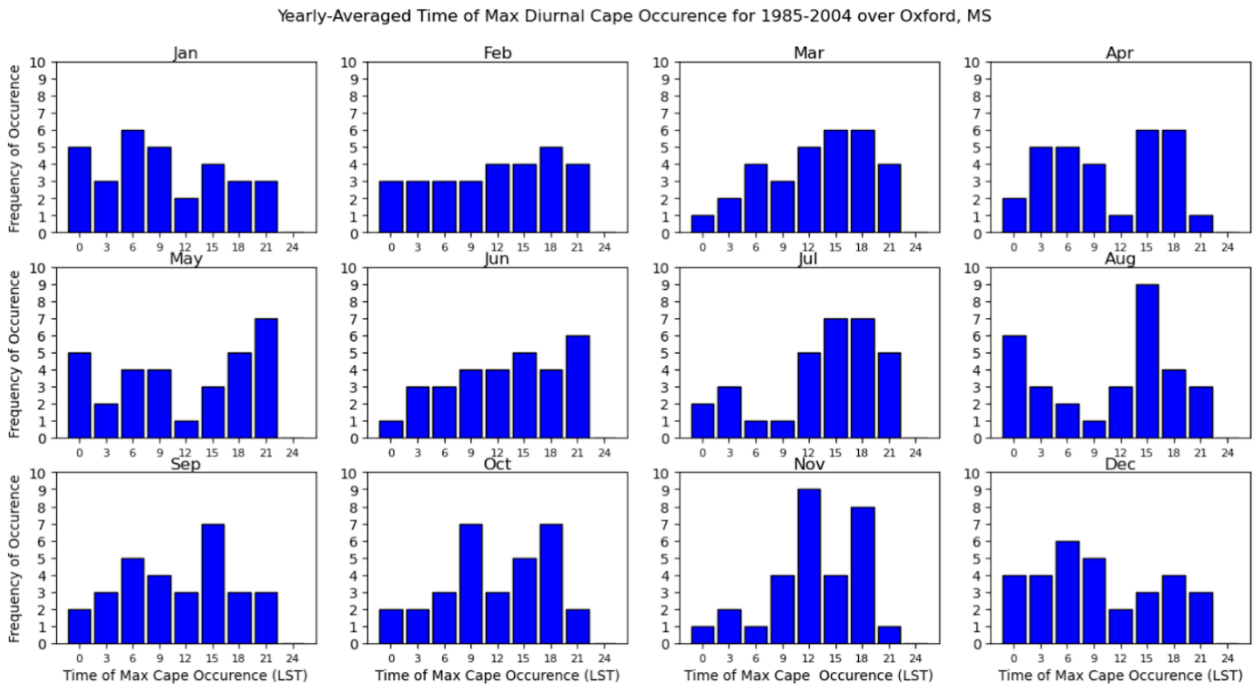

Figure 14: The time of day at which the maximum diurnal CAPE value occurred for every day of the month averaged over 20 years for Oxford, Mississippi.

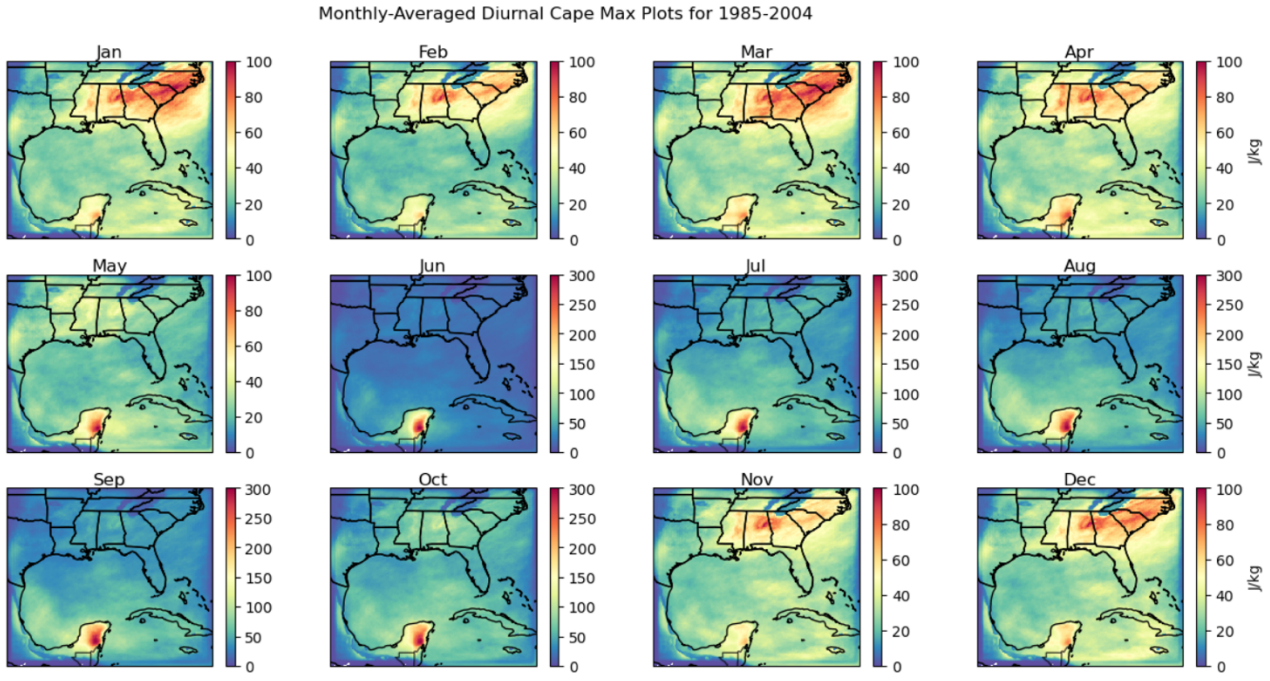

Figure 15: The monthly climatology of the diurnal maximum in CAPE from FLAReS1.0.

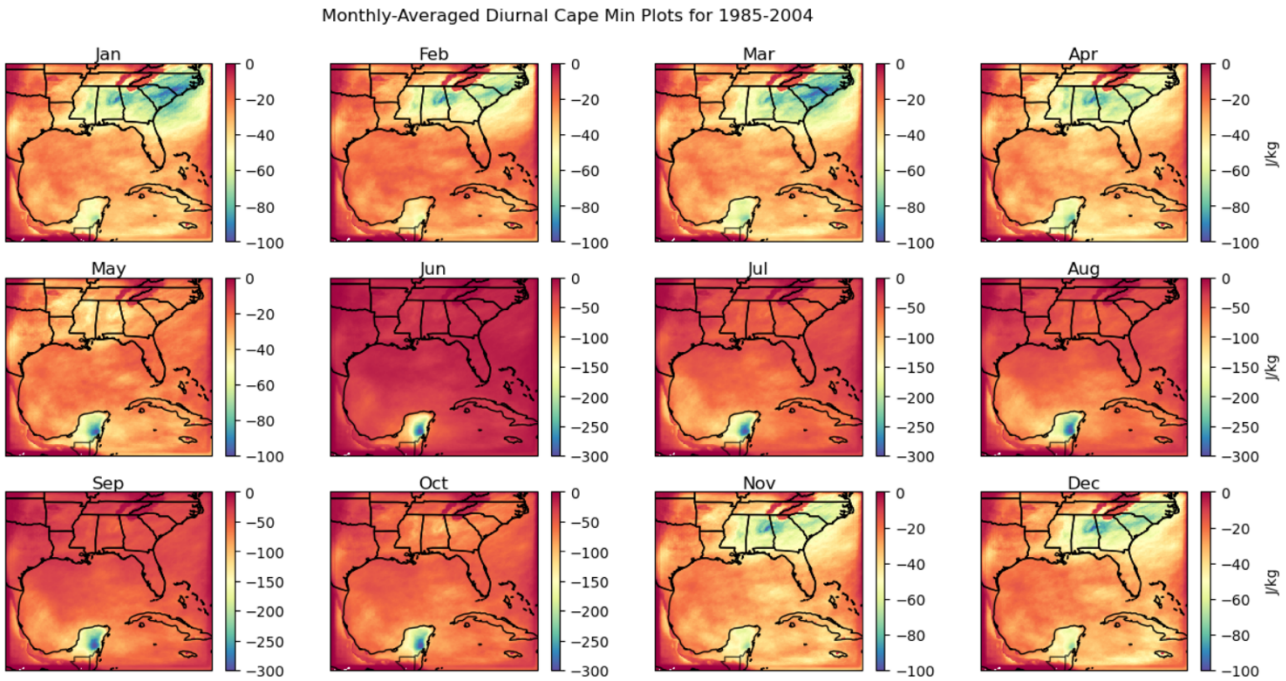

Figure 16: The monthly climatology of the diurnal minimum in CAPE from FLAReS1.0.